Significant difference in the dynamics between strong and fragile glass formers

Akira Furukawa* and Hajime Tanaka
Institute of Industrial Science, University of Tokyo, Meguro-ku, Tokyo 153-8505, Japan
(Received 17 September 2015; published 17 November 2016)

Glass-forming liquids are often classified into strong glass formers with nearly Arrhenius behavior and fragile ones with super-Arrhenius behavior. We reveal a significant difference in the dynamics between these two types of glass formers through molecular dynamics simulations: In strong glass formers, the relaxation dynamics of density fluctuations is nondiffusive, whereas in fragile glass formers it exhibits diffusive behavior. We demonstrate that this distinction is a direct consequence of the fundamental difference in the underlying elementary relaxation process between these two dynamical classes of glass formers. For fragile glass formers, a density-exchange process proceeds the density relaxation, which takes place locally at the particle level in normal states but is increasingly cooperative and nonlocal as the temperature is lowered in supercooled states. On the other hand, in strong glass formers, such an exchange process is not necessary for density relaxation due to the presence of other local relaxation channels. Our finding provides a novel insight into Angell's classification scheme from a hydrodynamic perspective.

DOI: 10.1103/PhysRevE.94.052607

I. INTRODUCTION

Despite considerable effort over many decades, the nature of the glass transition is still puzzling, with many unexplained phenomena and effects [1–6]. The most fundamental problem is why the viscosity η or the structural relaxation time τ_α increases dramatically on approaching the glass transition temperature T_g. However, not only does the origin of this dramatic viscous slowdown remain a mystery, but also there is still no general way to describe the anomalous relaxation dynamics in supercooled or glassy liquids. Recent intensive experimental and simulation studies have shown that the slowdown of the dynamics is associated with spatially correlated motions or structures (see Refs. [5–10] and references therein). Although most studies suggest the significance of such correlations, there is no consensus on their precise roles in the anomalous hydrodynamic transport of supercooled liquids; namely, we have not yet clearly understood the physical significance of these correlations, and, furthermore, we do not know how to relate the physical quantities or observables used for probing the spatial correlations to the hydrodynamic transport coefficients, most importantly, the viscosity anomaly.

Recently we have revealed [11–14] strong effects of spatial correlation on hydrodynamic transport: In supercooled states, both the (longitudinal) density diffusion and the (transverse) viscous relaxation exhibit a distinct crossover between microscopic and macroscopic transport, which characterizes the correlation length of the nonlocal hydrodynamic transport ξ. On the basis of the simulation results, it was argued [14] that a transiently correlated structure with the characteristic size ξ sustains long-lived stress and determines the nature of hydrodynamic transport. A natural question here is how general the above conclusion is. In all the above-mentioned simulation studies [11–14], we employed a prototype fragile glass former, the Bernu-Hiwatari-Hansen (BHH) soft-sphere model [15]. However, it is widely recognized that the slowdown behavior while approaching T_g is not universal. According to Angell's classification scheme [16], glass-forming liquids can be categorized into two classes: "strong" and "fragile" glass formers. Strong glass formers show nearly Arrhenius temperature dependence of the viscosity. The most typical examples are SiO_2 and GeO_2, which have network structures of (directional) covalent bonds. In fragile glass formers, on the other hand, the viscosity increases much steeper than the Arrhenius law near T_g. A widely accepted view on this distinction is as follows: The molecular motion of strong glass formers is less cooperative and controlled by temperature-independent (rather local) activation energy, thus leading to Arrhenius behavior. In fragile glass formers, on the other hand, growing cooperativity of molecular motion on cooling leads to super-Arrhenius behavior. Indeed, recent simulation studies support this scenario by indicating a close link between the fragility and the degree of dynamic heterogeneity [17–21]. However, there has so far been little study on the distinction between fragile and strong glass formers from a hydrodynamic viewpoint, despite the fact that the key transport in supercooled liquids is of hydrodynamic nature.

In this paper, we reveal a further fundamental distinction between strong and fragile glass-formers by use of a hydrodynamic approach, more specifically, by systematically investigating the length-scale-dependent dynamics of density fluctuations, and discuss its consequences for the relaxation dynamics.

II. SIMULATION MODELS

In this study, we used three simple and popular model glass-forming binary mixtures: a model for strong glass formers, the van Beest-Kramer-van Santen (BKS) [22] model, and two models for fragile glass-formers, the Kob-Andersen (KA) [23] and the Bernu-Hiwatari-Hansen (BHH) soft-sphere [15] models. All of these models were simulated using velocity Verlet algorithms in the NVE (constant number of particles, volume, and energy) ensemble [24]. Here, we describe the details of these model systems.

*Corresponding author: furu@iis.u-tokyo.ac.jp

A. The strong BKS model

The BKS model has been extensively studied to investigate structural and dynamical properties of amorphous and supercooled silica (SiO_2) [17,25–30], which is the prototype of strong glass formers. In Refs. [27,28], various aspects of the dynamics of density fluctuations were intensively studied. As shown below, our simulations at longer length and time scales may complement the results of Refs. [27,28].

The interaction potential of the BKS model is given by

$$U_{\mu\nu}^{\rm BKS}(r) = \frac{q_\mu q_\nu e^2}{r} + A_{\mu\nu}\exp(-B_{\mu\nu}r) - \frac{C_{\mu\nu}}{r^6}, \qquad (1)$$

where r is the distance between two ions and $\mu,\nu =$ Si, O. According to Refs. [22,25], the parameters are given as follows: $A_{\rm SiSi} = 0$ (eV), $A_{\rm SiO} = 18003.7572$ (eV), $A_{\rm OO} = 1388.7730$ (eV), $B_{\rm SiSi} = 0(\text{Å}^{-1})$, $B_{\rm SiO} = 4.87318(\text{Å}^{-1})$, $B_{\rm OO} = 2.76000(\text{Å}^{-1})$, $C_{\rm SiSi} = 0.0\,(\text{eV Å}^{-6})$, $C_{\rm SiO} = 133.5381\,(\text{eV Å}^{-6})$, and $C_{\rm OO} = 175.0000\,(\text{eV Å}^{-6})$. The partial charges are $q_{\rm Si} = 2.4$ and $q_{\rm Si} = -1.2$, and e^2 is given by $1602.19/4\pi 8.8542$ (eV Å). The Coulombic part is usually evaluated via the Ewald summation technique, which is time-consuming. Here, to reduce the computational cost, instead of using the original BKS model, we used its simplified version, in which the Coulombic interaction is approximated by the finite-range potential as [31,32]

$$\frac{q_\mu q_\nu e^2}{r} \to q_\mu q_\nu e^2\left[\left(\frac{1}{r} - \frac{1}{r_c}\right) + \frac{1}{r_c^2}(r - r_c)\right]. \qquad (2)$$

The potential is truncated at $r = r_c$ while satisfying the charge neutrality. In Ref. [32], it was shown that, with an appropriate choice of r_c, this treatment leads to a good quantitative agreement between the two cases of the truncated and nontruncated Coulombic interactions. In the present study, following Ref. [32], we set $r_c = 10.17$ (Å). The masses of the Si and O ions were $m_{\rm Si} = 4.6638 \times 10^{-23}$ (g) and $m_{\rm O} = 2.6568 \times 10^{-23}$ (g), respectively. We fixed the mass density at a value of 2.37 (g/cm^3). The unit length and time were $r_0 = 2.84$ (Å) and $t_0 = 1.98 \times 10^{-13}$ (s), respectively. The temperature was measured in units of 0.601 (eV)/$k_B = 6973.9$ (K), where k_B is the Boltzmann constant. For the main analysis, the total number of ions is $N = N_{\rm Si} + N_{\rm O} = 27\,000$ with $N_{\rm O}/N_{\rm Si} = 2$. Thus, the particle number density is $N/V = 1.632$, and the linear dimension of the system is $L = 25.48$ (corresponding to 72.36 Å). Additionally, to determine whether a diffusive relaxation of the density fluctuations is observable for a larger system size, we performed preliminary simulations with the values of $N = 432\,000$ and $L = 64.21(182.3$ Å) (see Fig. 2).

B. The fragile KA model

The KA model [23] is a binary mixture, which is composed of large (A) and small (B) particles of equal masses, $m_A = m_B = m$. The interaction potential is given by

$$U_{\mu\nu}^{\rm KA}(r) = 4\epsilon_{\mu\nu}\left[\left(\frac{\lambda_{\mu\nu}}{r}\right)^{12} - \left(\frac{\lambda_{\mu\nu}}{r}\right)^{6}\right] - U_{\mu\nu}^0, \qquad (3)$$

where $\mu,\nu = A,B$, $\epsilon_{AB} = 1.5\epsilon_{AA}$, $\epsilon_{BB} = 0.5\epsilon_{AA}$, $\lambda_{AB} = 0.8\lambda_{AA}$, and $\lambda_{BB} = 0.88\lambda_{AA}$ and r is the distance between two particles. The potential is truncated at $r = 2.5\lambda_{\mu\nu}$ and

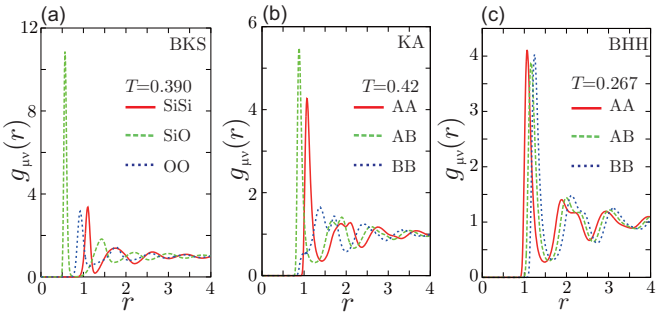

FIG. 1. The radial distribution function $g_{\mu\nu}(r)$ in a supercooled state for the BKS (a), KA (b), and BHH (c) models.

$U_{\mu\nu}^0$ is chosen to satisfy $U_{\mu\nu}^{\rm KA}(2.5\lambda_{\mu\nu}) = 0$. The temperature T was measured in units of ϵ_{AA}/k_B. We held the particle number density constant at a value of $N/V = 1.2/\lambda_A^3$, where $N = N_A + N_B = 36\,000$ with $N_A/N_B = 4$, and V is the system volume. The space and time units were λ_{AA} and $(m\lambda_{AA}^2/\epsilon_{AA})^{1/2}$, respectively. Then, the linear dimension of the system was $L = 31.07$.

C. The fragile BHH model

The Bernu-Hiwatari-Hansen model [15] is a binary mixture of large (A) and small (B) particles interacting via the soft-core potentials

$$U_{\mu\nu}^{\rm BHH}(r) = \epsilon\left(\frac{\lambda_{\mu\nu}}{r}\right)^{12}, \qquad (4)$$

where $\mu,\nu = A,B$, $\lambda_{\mu\nu} = (\lambda_\mu + \lambda_\nu)/2$, λ_μ is the particle size, and r is the distance between two particles. The mass and size ratios are $m_B/m_A = 2$ and $\lambda_B/\lambda_A = 1.2$, respectively. The units for the length and time are λ_A and $(m_A\lambda_A^2/\epsilon)^{1/2}$, respectively. The total number of particles was $N = N_A + N_B = 40\,000$ and $N_A/N_B = 1$. The temperature T was measured in units of ϵ/k_B. The fixed particle number density and the linear dimension of the system were $N/V = 0.8/\lambda_A^3$ and $L = 36.84$, respectively.

In Sec. III C, the coordination number around the ith particle of the μ species, z_i^μ, will be defined as the number of particles satisfying $|\boldsymbol{r}_i^\mu(t) - \boldsymbol{r}_j^\nu(t)| < r_{\rm min}^{\mu\nu}$. As shown in Fig. 1, the radial distribution function, $g_{\mu\nu}(r)$, exhibits a clear minimum between the first and the second peaks at $r = r_{\rm min}^{\mu\nu}$, except for $g_{BB}(r)$ in the KA model. Thus, for the KA model, we set $r_{\rm min}^{BB} = 1.073\lambda_{AA}(= 1.219\lambda_{BB})$ at which $g_{BB}(r)$ has a plateau and $-U_{BB}^{\rm KA}(r_{\rm min}^{BB}) = 0.42$.

III. QUALITATIVE DIFFERENCE IN THE DYNAMICS

A. Difference in the density relaxation: Nondiffusive (strong) vs. diffusive (fragile) relaxation

First, to reveal the nature of the dynamics of density fluctuations, we study the wave number (k) dependence of the relaxation time of the number-density fluctuations, $\tau_n(k)$, for the three systems. We determine $\tau_n(k)$ by fitting a stretched exponential function $A_k\exp\{-[t/\tau_n(k)]^{\beta_k}\}$, where A_k and β_k are the k-dependent coefficient and exponent, respectively, to the long-time ($t \gtrsim \tau_\alpha$) decay of the scaled

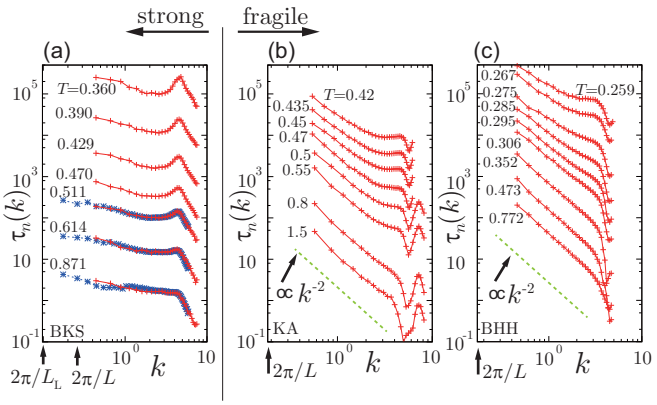

FIG. 2. The k dependence of the relaxation time of the number density fluctuations, $\tau_n(k)$, at various temperatures for the BKS (a), KA (b), and BHH (c) models. In the BKS model, density fluctuations do not exhibit diffusive behavior but relax with almost the same time scale over a significant k range. In the KA and BHH models, on the other hand, the relaxation dynamics is diffusive at longer length scales: $\tau_n(k) \sim k^{-2}$. In the BKS model, we also show the results for the larger system ($L_L = 2.52L$) at the three higher temperatures by the blue dashed curves. Even at this larger system size, we do not observe diffusive behavior in the density relaxation [33].

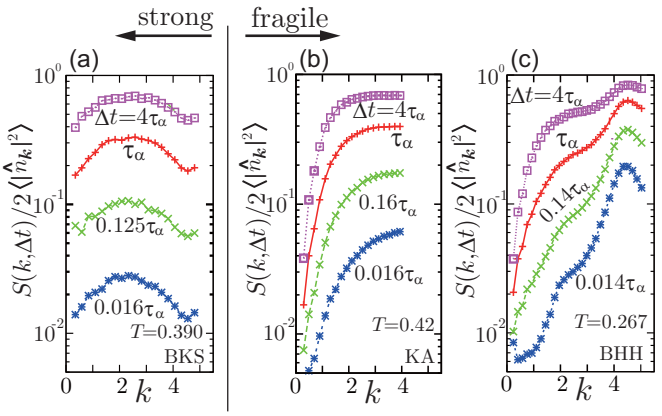

FIG. 3. $S(k,\Delta t) = \langle|\Delta\hat{n}_{\boldsymbol{k}}(\Delta t)|^2\rangle/N$ scaled by $2\langle|\hat{n}_{\boldsymbol{k}}|^2\rangle/N$ for the BKS (a), KA (b), and BHH (c) models in supercooled states. Note that $\lim_{\Delta t\to\infty} S(k,\Delta t) = 2\langle|\hat{n}_{\boldsymbol{k}}|^2\rangle/N$.

autocorrelation function, $G(k,t) = \langle n_{\boldsymbol{k}}(t)n_{-\boldsymbol{k}}(0)\rangle/\langle|n_{\boldsymbol{k}}|^2\rangle$. Here, $n_{\boldsymbol{k}} = \sum_i^N e^{-i\boldsymbol{k}\cdot\boldsymbol{r}_i}$ is the Fourier space representation of the particle number density and $\boldsymbol{r}_i$ is the position vector of the ith particle. Hereafter, $\langle\cdots\rangle$ denotes the ensemble average and $f_{\boldsymbol{k}}$ is defined as the Fourier transform of an arbitrary field variable $f(\boldsymbol{r})$. Figure 2 shows the k dependence of $\tau_n(k)$ for the three models at various temperatures T, indicating distinct differences in density relaxation between strong and fragile glass formers: In the strong BKS model, density fluctuations do not exhibit diffusive k dependence but relax in the time scale of τ_α [$\tau_n(k) \sim \tau_\alpha$] independently of k over the whole k-range of the present study. We note that τ_α is defined as the macroscopic stress relaxation time (see Fig. 7 in the Appendix A). Note that in Ref. [27], the nondiffusive behavior of the relaxation times were also found, but the calculations were performed at microscopic scales ($k \gtrsim 3.1$ in our units). In fragile glass formers, on the other hand, the relaxation dynamics exhibits diffusive nature at longer length scales, satisfying $\tau_n(k) \sim k^{-2}$.

This difference can also be seen by looking at the spatial correlation of the temporal density change over a time period Δt. To do so, we calculate $S(k,\Delta t) = \langle|\Delta\hat{n}_{\boldsymbol{k}}(\Delta t)|^2\rangle/N$ scaled by $2\langle|\hat{n}_{\boldsymbol{k}}|^2\rangle/N$, where $\Delta\hat{n}_{\boldsymbol{k}} = \hat{n}_{\boldsymbol{k}}(\Delta t) - \hat{n}_{\boldsymbol{k}}(0)$. To exclude the effects of short-term vibrations, we use the time-averaged density defined as $\hat{n}_{\boldsymbol{k}}(t) = (1/\delta t)\int_t^{t+\delta t} ds\, n_{\boldsymbol{k}}(s)$. Here, we set $\delta t = 0.005\tau_\alpha$, but our results are insensitive to the choice of δt, as long as $\tau_0 \ll \delta t \ll \tau_\alpha$, where τ_0 is a typical microscopic vibration time. $S(k,\Delta t)$ measures the k dependence of the magnitude of the temporal change of the Fourier mode of density fluctuations. Figure 3 shows $S(k,\Delta t)$ for the three systems. In the KA and BHH models, the temporal growth of the fluctuations of $\Delta\hat{n}_{\boldsymbol{k}}$ at smaller k is highly suppressed. In the BKS model, on the other hand, the density change occurs with almost the same time scale for any k. As further discussed below, these results indicate the diffusive and nondiffusive natures of density fluctuations in fragile and strong glass formers, respectively. Note that this nondiffusive nature of strong glass formers at finite k does not mean the presence of macroscopic ($k = 0$) density fluctuation, which is, of course, prohibited.

B. Difference in the longitudinal displacement: Vibrational (strong) vs. diffusive (fragile) displacement at the time scale of τ_α

Different aspects of this distinction can be found in the spatial correlation of longitudinal displacement vectors. Figure 4 shows the plot of $H(k,\Delta t) = \langle|\boldsymbol{k}\cdot\hat{\boldsymbol{u}}_{\boldsymbol{k}}(\Delta t)|^2\rangle/N$, where $\hat{\boldsymbol{u}}_{\boldsymbol{k}}(\Delta t) = \sum_i^N \boldsymbol{u}_i(\Delta t)e^{-i\boldsymbol{k}\cdot\boldsymbol{r}_i}$ and $\boldsymbol{u}_i(\Delta t) = \boldsymbol{r}_i(\Delta t) - \boldsymbol{r}_i(0)$ is the displacement vector of ith particle for the time duration Δt. For $\Delta t \ll \tau_\alpha$, $i\boldsymbol{k}\cdot\hat{\boldsymbol{u}}_{\boldsymbol{k}}$ approximately represents the thermally fluctuating (volumetric) elastic strain fields. Therefore, for both strong and fragile glass formers, $H(k,\Delta t)$ has a flat k dependence as $H(k,\Delta t) \sim T/K_B$ at smaller k, where K_B is the (k independent) bulk modulus. However, as Δt increases, the difference in $H(k,\Delta t)$ is more pronounced. For the strong BKS silica, even at the time scale of the structural relaxation

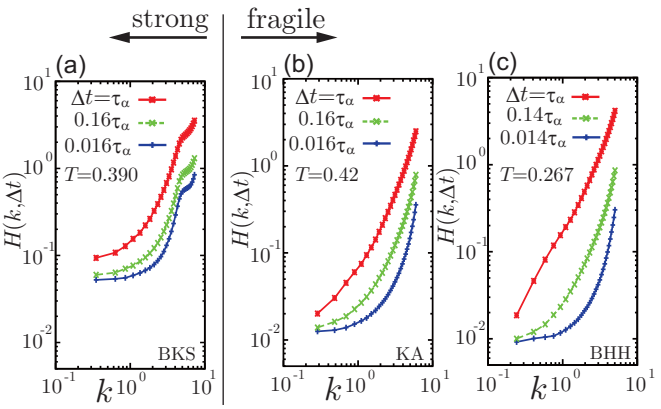

FIG. 4. $H(k,\Delta t) = \langle|\boldsymbol{k}\cdot\hat{\boldsymbol{u}}_{\boldsymbol{k}}(\Delta t)|^2\rangle/N$ for the BKS (a), KA (b), and BHH (c) models in supercooled states. Here, $\hat{\boldsymbol{u}}_{\boldsymbol{k}}(\Delta t) = \sum_i^N \boldsymbol{u}_i(\Delta t)e^{-i\boldsymbol{k}\cdot\boldsymbol{r}_i}$ and $\boldsymbol{u}_i(\Delta t) = \boldsymbol{r}_i(\Delta t) - \boldsymbol{r}_i(0)$ is the displacement vector of ith particle for the time duration Δt.

($\sim \tau_\alpha$), $H(k,\Delta t)$ still shows a relatively weak k dependence for small k, indicating that the vibrational motions have important contributions to the longitudinal dynamics. In contrast, for the fragile glass formers, the diffusive displacements are already dominant at the same time scale [34]. We note that even for the BKS model, for the much longer time duration ($\Delta t \gg \tau_\alpha$), a clear k^2 dependence should also be recovered due to the diffusive displacement of particles; however, at this time regime, density fluctuations have already relaxed via local relaxation channels (see below). That is, the time scales between the stress relaxation and the diffusion (of n and $\boldsymbol{u}$) are significantly separated in the strong BKS model but are rather close in the fragile KA and BHH models.

This time separation in the BKS model can be explained as follows: In supercooled silica, the covalent Si-O bond is very stable and, on average, survives for a period longer than τ_α, so the structural relaxation mainly proceeds by rotational rearrangements of SiO_4 tetrahedra around nearly immobile Si. For this time duration, the longitudinal displacements still fluctuate closely around the initial value. This type of structural relaxation process was predicted by Buchenau *et al.* [35] based on the experimental results and later numerically confirmed by Saksaengwijit and Heuer [29]. Moreover, in Ref. [28], a close link between density and transverse-current spectra was shown at relatively short time scales, which indicated the relevant dynamic coupling between density fluctuations and rotations of SiO_4 tetrahedra. We speculate that the long-term effect of this dynamic coupling contributes significantly to the relaxation of density fluctuations.

C. Difference in the elementary process: Without (strong) vs. with (fragile) density-exchange

Now we seek the physical origin for the above difference between strong and fragile glass formers. For this purpose, we investigate the local correlation of the coordination-number change. In these binary mixtures, the coordination number of the ith particle of the μ species at time t, $z_i^\mu(t)$, is defined as the number of particles satisfying $|\boldsymbol{r}_i^\mu(t) - \boldsymbol{r}_j^\nu(t)| < r_{\min}^{\mu\nu}$. At $r = r_{\min}^{\mu\nu}$, the radial distribution function $g_{\mu\nu}(r)$ has its first minimum (see Sec. II). In Fig. 5(a), we show the correlation function $G_{\mu\nu}(r;\Delta t)$ defined as

$$G_{\mu\nu}(r;\Delta t) = \frac{\sum_{i=1}^{N_\mu}\sum_{j=1}^{N_\nu}\left\langle \Delta z_i^\mu \Delta z_j^\nu \delta\left(r - |\boldsymbol{r}_i^\mu(t) - \boldsymbol{r}_j^\nu(t)|\right)\right\rangle}{4\pi r^2 n_\mu n_\nu V},$$

where $\Delta z_i^\mu = z_i^\mu(t+\Delta t) - z_i^\mu(t)$, V is the system volume, and $n_{\mu(\nu)} = N_{\mu(\nu)}/V$ with $N_{\mu(\nu)}$ being the number of $\mu(\nu)$-species particles. In Fig. 5(b), we plot $\Gamma_\mu(r;\Delta t) = \sum_\nu (n_\nu/n) G_{\mu\nu}(r;\Delta t)$ at $\Delta t = \tau_\alpha$. Here, $n = \sum_\mu n_\mu$ is the total number density. $\Gamma_\mu(r;\Delta t)$ represents the correlation of the coordination-number change for a given μ-species particle. In the fragile KA and BHH models, $\Gamma_\mu(r;\Delta t)$ exhibits negative and positive correlations in the first shell and its outer shells, respectively, indicating a mutual density exchange between nearest neighbors. That is, when an increase or a decrease of the surrounding particles occurs, the opposite happens simultaneously at the nearest-neighbor particles (the local density conservation). In contrast, in the strong BKS model, only positive correlations are observed. Thus, an increase or a decrease in the surrounding particles occurs (rather freely) without such mutual exchange processes; more specifically, a local density change is induced by the creation or annihilation of defective O-O pairs via rearrangements of SiO_4 tetrahedra. As a consequence of this clear difference in the elementary process, for the length scales of interest, the fragile glass formers express the diffusive (conservative) dynamics, while in the strong BKS model, density fluctuations behave as though they were nonconserved variables, resulting in the nondiffusive dynamics in the accessible k range; that is, the diffusive (conservative) and nondiffusive (nonconservative) dynamics of fragile and strong glass formers are the hydrodynamic manifestations of the presence and absence of the mutual density exchange, respectively [36].

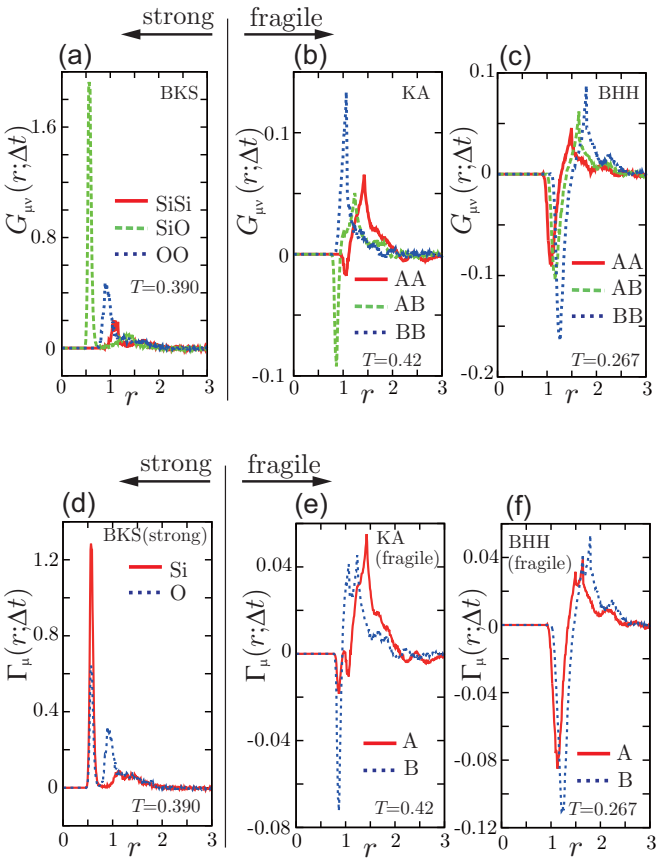

FIG. 5. Upper panel: $G_{\mu\nu}(r;\Delta t)$ for a $\mu\nu$ pair for the BKS (a), KA (b), and BHH (c) models. Lower panel: $\Gamma_\mu(r;\Delta t) = \sum_\nu (\rho_\nu/\rho) G_{\mu\nu}(r;\Delta t)$ for the BKS (d), KA (e), and BHH (f) models. Here, $\Delta t = \tau_\alpha$. See Sec. II for the definition of the species index.

Our study suggests that, in strong glass formers, a local density change (volume expansion or contraction) occurs more easily than in fragile glass formers, and therefore, strong glass formers are more compressible than fragile glass formers even in the time scale of the α relaxation [38]. This situation may be a consequence of the significantly lower packing density of the BKS model than the two fragile models. Such a correlation between the atomic packing density and the fragility and its influence on the mechanical properties has been recognized [42–45]: In general, strong glass formers have a lower Poisson's ratio and a lower packing density than fragile

glass formers. Also importantly, strong glass formers typically exhibit brittle-type fracture behavior, whereas fragile glass formers show a ductile one [45]. The above results suggest that the density and longitudinal stress fluctuations should be more easily enhanced in stronger glass formers, leading to weaker resistance to volumetric deformation and resulting in more catastrophic failure. Further investigations are necessary for a quantitative understanding of the correlation between fragility and mechanical properties.

IV. LENGTH-SCALE-DEPENDENT DIFFUSION IN THE FRAGILE GLASS-FORMERS

We show in the above that the relaxation dynamics is always rather local and nondiffusive for strong glass formers and the relaxation mechanism is insensitive to the degree of supercooling within the temperature range studied here. For fragile glass formers, on the other hand, the degree of cooperativity changes with an increase in the degree of supercooling. Here, for the fragile KA and BHH models, we discuss this problem in more detail by analyzing the k-dependent density-diffusion coefficient $D_n(k)$, which is generally defined by $D_n(k) = 1/[k^2\tau_n(k)]$. The macroscopic density-diffusion coefficient is formally identified as $D_n = \lim_{k\to 0} D_n(k)$. In normal liquid states at higher temperatures, particle-scale dynamics dominates hydrodynamic transport. The structural relaxation takes place by particle exchange between nearest neighbors over the distance of the particle size λ, leading to the following expression of the density-diffusion coefficient: $D_n \sim \lambda^2/\tau_\alpha$ [13,14]. This relation is nothing but the Stokes-Einstein relation, which describes single-particle self-diffusion in normal liquid states [46–48]. However, as the temperature is lowered, this particle-scale dynamics should be surpassed by cooperative dynamics associated with a growing correlation length ξ of the nonlocal hydrodynamic transport. This can be seen in Fig. 6(a), which shows the k dependence of the diffusion coefficient $D_n(k)$ scaled by $T/\eta(\sim 1/\tau_\alpha)$. Here, the particle size λ is set to the unit length. At higher temperatures (in normal liquid states), $D_n(k)$ shows a constant diffusivity $[D_n(k) \sim T/\eta]$ for length scales larger than the particle size. However, as the degree of supercooling increases, the deviation from this constant diffusivity is enhanced. As described in Ref. [14], in supercooled states, the collective density relaxation can be viewed as a consequence of the diffusion of transiently correlated fluctuations of size ξ in a medium with macroscopic viscosity η. This physical picture leads to the following expression of D_n:

$$D_n \sim \xi^2/\tau_\alpha (\gg \lambda^2/\tau_\alpha).$$

To confirm the relevance of this picture, we show in Fig. 6(b) the diffusion coefficient $D_n(k)$ scaled by $T\xi^2/\eta(\sim \xi^2/\tau_\alpha)$ instead of by T/η in supercooled states as a function of the scaled wave number $k\xi$. Here, ξ is identified as the correlation length of the nonlocal hydrodynamic transport determined by the k dependence of the shear viscosity (see the Appendix B). We find that $D_n(k)/(T\xi^2/\eta)$ falls onto nearly a single master curve; $D_n(k)/(T\xi^2/\eta) \sim 1$ for $k\xi \lesssim 1$, while $D_n(k)/(T\xi^2/\eta) \sim 1/(k\xi)^2$ for $k\xi \gtrsim 1$. This observation can be understood as follows. For $k\xi \lesssim 1$, the slowly relaxing density fluctuations obey the diffusion equation with a diffusion coefficient $T\xi^2/\eta$. On the other hand, for $k\xi \gtrsim 1$, the relaxation time, $1/[D_n(k)k^2]$, is nearly equal to the α-relaxation time $\tau_\alpha \propto \eta/T$; thus, the density fluctuations survive for the time scale of $\tau_n(k) \sim \tau_\alpha$. These observations strongly support that the crossover from particle-scale dynamics to cooperative dynamics occurs in the density diffusion for fragile glass formers.

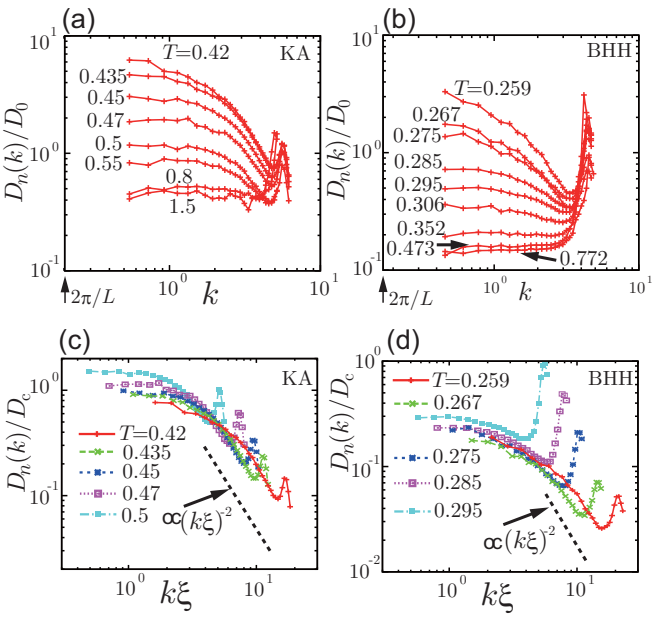

FIG. 6. Upper panel: The behavior of $D_n(k)$ scaled by $D_0 = T/\eta$ as a function of k for the KA (a) and BHH (b) models. Lower panel: The behavior of $D_n(k)$ scaled by $D_c = T\xi^2/\eta \sim \xi^2/\tau_\alpha$ as a function of $k\xi$ for the KA (c) and BHH (d) models.

V. CONCLUDING REMARKS

In conclusion, we have found a fundamental difference in the dynamics between strong and fragile glass formers. In strong glass formers, density fluctuations relax rather locally, whereas in fragile glass formers they relax cooperatively via diffusion. Furthermore, we have shown that this distinction can be attributed to the essential difference in the underlying relaxation process: In strong glass formers, the density and structural relaxations can proceed locally by vibrational or rotational displacements, while in fragile glass formers they require diffusive displacements. For the latter, because of the low compressibility, the density fluctuations are strongly suppressed at larger length scales in the time scale of the structural relaxation. We have also discussed the change in the mechanism of the density diffusion in fragile glass formers, based on a simple scaling argument. We note that our preliminary simulations for other different model glass formers (not shown here) also follow the above-mentioned characteristics. Our result shows that the relaxation behavior (diffusive vs. nondiffusive) does not depend on the temperature or the degree of supercooling, suggesting that it originates from the intrinsic nature of material. This apparently contradicts a recent finding of the "fragile-to-strong" crossover in a prototype strong liquid silica [30]. Note, however, that the

observed relaxation behavior of the BKS model above the "crossover" temperature, which has been considered to be in a "fragile" state, is clearly distinct to those of the KA and BHH models. Including the meaning of fragile liquids far above T_g, this point is an interesting problem for future investigation.

ACKNOWLEDGMENTS

This work was supported by KAKENHI (Grants No. 26103507, No. 25000002, and No. 20508139) and the JSPS Core-to-Core Program "International research network for non-equilibrium dynamics of soft matter."

APPENDIX A: MACROSCOPIC STRESS RELAXATION TIME

Here, the α-relaxation time, τ_α, is defined as the macroscopic stress relaxation time that is determined by the shear stress autocorrelation function, $H(t) = \langle \hat{\sigma}_{xy}(t)\hat{\sigma}_{xy}(0)\rangle / VT$, where $V = L^3$ is the system volume and $\hat{\sigma}_{xy}$ is the xy component of the shear stress tensor that is given by

$$\hat{\boldsymbol{\sigma}} = \sum_i \left[m_i \boldsymbol{v}_i \boldsymbol{v}_i - \frac{1}{2} \sum_{j \neq i} \frac{\boldsymbol{r}_{ij}\boldsymbol{r}_{ij}}{r_{ij}} \frac{\partial U_{ij}}{\partial r_{ij}} \right]. \tag{A1}$$

Here, $\boldsymbol{r}_{ij} = \boldsymbol{r}_i - \boldsymbol{r}_j$, $r_{ij} = |\boldsymbol{r}_{ij}|$, and m_i and $\boldsymbol{v}_i$ are the mass and velocity of the ith particle, respectively. The first term in Eq. (A1) represents the momentum transfer contribution (ideal-gas term), which is negligibly small in comparison to the second term in the high-density liquid. The time integration of $H(t)$ gives the macroscopic shear viscosity: $\eta = \int_0^\infty dt\, H(t)$. We determined τ_α by fitting the long-time behavior of $H(t)$ to the Kohlrausch-Williams-Watts form, $G_0 \exp[-(t/\tau_\alpha)^\psi]$, where G_0 is the plateau modulus, and ψ is the exponent of nonexponential decay. In Fig. 7, we plot the temperature dependence of τ_α for the BKS, KA, and BHH models. In the strong BKS model, τ_α exhibits an Arrhenius behavior. However, in the fragile KA and BHH models, τ_α shows a non-Arrhenius temperature dependence, which can be fitted to the Vogel-Fulcher-Tamman (VFT) law.

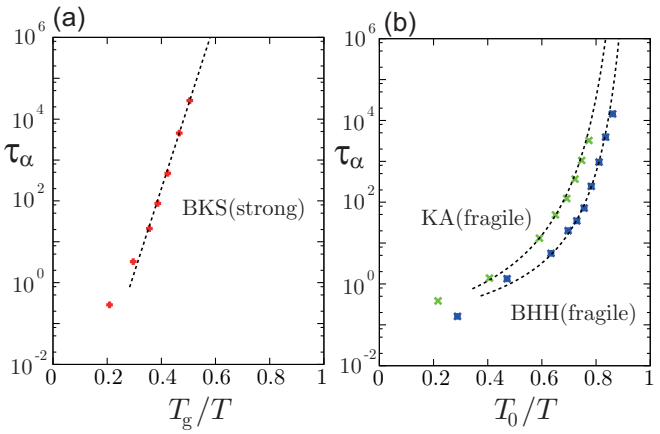

FIG. 7. The temperature dependence of τ_α for the three models. (a) For the strong BKS model, τ_α is plotted against T_g/T. At lower temperatures, τ_α can be fitted to the Arrhenius form, $\tau_0 \exp(E/T)$ (dashed curve), where $\tau_0 = 1.18 \times 10^{-6}$ and $E = 8.61$. The glass transition temperature, $T_g(= 0.182)$, is estimated as the temperature at which $\tau_\alpha = 100$(s) (corresponding to 5.05×10^{14} in our units). This empirical determination of T_g is often used in experimental studies [16]. (b) For the fragile KA and BHH models, τ_α is plotted against T_0/T. At lower temperatures, τ_α follows the VFT law, $\tau_\alpha = \tau_0 \exp[K/(T/T_0 - 1)]$ (dashed curve). Here, $\tau_0 = 0.15(0.15)$, $K = 3.1(2.05)$, and the VFT temperature is $T_0 = 0.325(0.223)$ for the KA(BHH) model. The K is the fragility index, representing the degree of deviation from the Arrhenius law; more fragile glass formers have larger values of K^{-1}.

APPENDIX B: THE k-DEPENDENT VISCOSITY IN THE KA AND BHH MODELS

For the fragile KA and BHH models, the slowly relaxing density fluctuations can be characterized by the correlation length of the hydrodynamic transport, as determined by the wave number (k) dependence of the shear viscosity $\eta(k)$. Here, we first describe the general formalism used to obtain $\eta(k)$ and then show the results for the KA and BHH models.

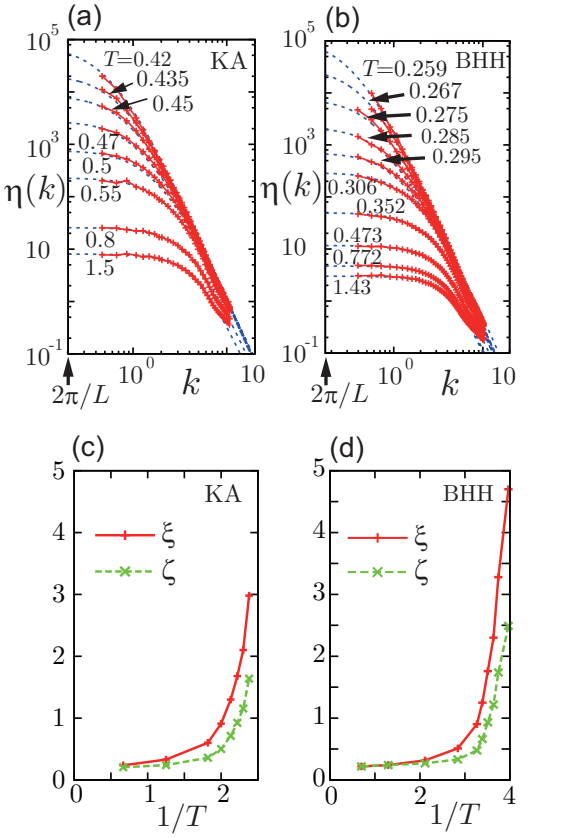

FIG. 8. Upper panel: The k dependence of the shear viscosity, $\eta(k)$, for the KA (a) and BHH (b) models at several temperatures. The blue dashed curve represents the empirical fitting function, $\eta/[1 + (\xi k)^2 + (\zeta k)^4]$, where η is the macroscopic ($k = 0$) viscosity determined by the Green-Kubo formula. Lower panel: The temperature dependence of the characteristic length scales, ξ and ζ, for the KA (c) and BHH (d) models. The former is the correlation length of the nonlocal viscous response.

We start from the following generalized hydrodynamic equation [46,47]:

$$\frac{\partial}{\partial t}\boldsymbol{j}^{\perp} = (\nabla \cdot \overleftrightarrow{\boldsymbol{\sigma}}_{\rm vis})^{\perp} + \boldsymbol{\theta}^{\perp}, \tag{B1}$$

where $\boldsymbol{j}^{\perp}(\boldsymbol{r},t)$ is the transverse-momentum current, $\boldsymbol{\theta}^{\perp}(\boldsymbol{r},t)$ is the transverse random force, and $\overleftrightarrow{\boldsymbol{\sigma}}_{\rm vis}(\boldsymbol{r},t)$ is the (transverse) viscous shear stress tensor that is given by $\overleftrightarrow{\boldsymbol{\sigma}}_{\rm vis}(\boldsymbol{r},t) = \int dt' \int d\boldsymbol{r}' \eta(|\boldsymbol{r}-\boldsymbol{r}'|,t-t') \overleftrightarrow{\boldsymbol{\kappa}}^{\perp}(\boldsymbol{r}',t')$ with a strain rate tensor of $\overleftrightarrow{\boldsymbol{\kappa}}^{\perp}(\boldsymbol{r},t) = \nabla \boldsymbol{v}^{\perp} + (\nabla \boldsymbol{v}^{\perp})^{\dagger}$. Here, $\boldsymbol{v}^{\perp}(\boldsymbol{r},t)$ is the transverse velocity, and $\eta(|\boldsymbol{r}-\boldsymbol{r}'|,t-t')$ is a response function that represents the spatiotemporal nonlocal viscoelastic response. In the k space, the above equation is expressed as

$$\frac{\partial}{\partial t}\boldsymbol{j}_{\boldsymbol{k}}{}^{\perp}(t) = -\frac{k^2}{\rho_{\rm m}} \int dt' \eta(k,t-t') \boldsymbol{j}_{\boldsymbol{k}}^{\perp}(t') + \boldsymbol{\theta}_{\boldsymbol{k}}^{\perp}(t), \tag{B2}$$

where ρ_m is the average mass density. Here, the Fourier transform of an arbitrary function, $f(\boldsymbol{r})$, is defined by $f_{\boldsymbol{k}} = \int d\boldsymbol{r} e^{-i\boldsymbol{k}\cdot\boldsymbol{r}} f(\boldsymbol{r})$. The microscopic expression of $\boldsymbol{j}_{\boldsymbol{k}}^{\perp}(t)$ is given by $\boldsymbol{j}_{\boldsymbol{k}}^{\perp}(t) = 1/\sqrt{N}\sum_i^N m_i \boldsymbol{v}_i^{\perp}(t) e^{i\boldsymbol{k}\cdot\boldsymbol{r}_i(t)}$, where $\boldsymbol{v}_i^{\perp}(t)$ is the transverse part of the velocity of particle i and thus satisfies $\boldsymbol{v}_i^{\perp}(t)\cdot\boldsymbol{k} = 0$. Then, the autocorrelation function is defined as $C(k,t) = \langle \boldsymbol{j}_{\boldsymbol{k}}^{\perp}(t)\cdot\boldsymbol{j}_{-\boldsymbol{k}}^{\perp}(0)\rangle$, whose time evolution is described by $(\partial/\partial t)C(k,t) = -(k^2/\rho_{\rm m})\int dt' \eta(k,t-t')C(k,t')$. Here, we make use of the relation $\langle \boldsymbol{\theta}_{\boldsymbol{k}}^{\perp}(t)\cdot\boldsymbol{j}_{-\boldsymbol{k}}^{\perp}(t')\rangle = 0$. The resulting (k,ω) dependence of the shear viscosity can be expressed as

$$\eta(k,\omega) = \frac{\rho_{\rm m}}{k^2\tilde{C}(k,\omega)}[-i\omega\tilde{C}(k,\omega) + C(k,0)], \tag{B3}$$

where $\tilde{C}(k,\omega) = \int_0^{\infty} dt e^{-i\omega t} C(k,t)$. The nonlocal viscoelasticity is characterized by the complex shear modulus, $G^*(k,\omega) = G'(k,\omega) + iG''(k,\omega) = i\omega\eta^*(k,\omega)$, where $G'(k,\omega)$ and $G''(k,\omega)$ are the so-called storage and loss modulus, respectively. The storage modulus represents the elastic response, whereas the loss modulus represents the dissipative viscous response. In the low-frequency limit ($\omega \to 0$), the k-dependent shear viscosity is obtained as

$$\eta(k) = \lim_{\omega\to 0}\frac{G''(k,\omega)}{\omega} = \frac{\rho_{\rm m}}{k^2}\left[\int_0^{\infty} dt \frac{C(\boldsymbol{k},t)}{C(\boldsymbol{k},0)}\right]^{-1}. \tag{B4}$$

Figure 8(a) shows the k dependence of the shear viscosity for the KA and BHH models at several temperatures. At high-temperature normal-liquid states, $\eta(k)$ smoothly approaches its macroscopic ($k = 0$) value with a decrease in k already at a wavelengths comparable to the particle size. However, in supercooled states, $\eta(k)$ exhibits a distinct crossover between the microscopic and macroscopic transport at a length of ξ, as shown in Fig. 8(b). The same plot for the BHH models was previously reported in Refs. [11–14].

[1] M. D. Ediger, C. A. Angell, and S. R. Nagel, J. Phys. Chem. **100**, 13200 (1996).
[2] P. G. Debenedetti and F. H. Stillinger, Nature **410**, 259 (2001).
[3] K. Binder and W. Kob, *Glassy Materials and Disordered Solids* (World Scientific, Singapore, 2005).
[4] J. C. Dyre, Rev. Mod. Phys. **78**, 953 (2006).
[5] L. Berthier and G. Biroli, Rev. Mod. Phys. **83**, 587 (2011).
[6] *Dynamical Heterogeneities in Glasses, Colloids, and Granular Media*, edited by L. Berthier, G. Biroli, J-P. Bouchaud, L. Cipelletti, and W. van Saarloos (Oxford University Press, Oxford, 2011).
[7] H. Tanaka, Eur. Phys. J. E **35**, 113 (2012).
[8] *Structural Glasses and Supercooled Liquids: Theory, Experiment, and Applications*, edited by G. Wolynes and V. Lubchenko (Wiley, New York, 2012).
[9] L. Berthier and W. Kob, Phys. Rev. E **85**, 011102 (2012).
[10] C. Cammarota and G. Biroli, Proc. Natl. Acad. Sci. USA **109**, 8850 (2012).
[11] A. Furukawa and H. Tanaka, Phys. Rev. Lett. **103**, 135703 (2009).
[12] A. Furukawa and H. Tanaka, Phys. Rev. E **84**, 061503 (2011).
[13] A. Furukawa and H. Tanaka, Phys. Rev. E **86**, 030501(R) (2012).
[14] A. Furukawa, Phys. Rev. E **87**, 062321 (2013).
[15] B. Bernu, Y. Hiwatari, and J. P. Hansen, Phys. C: Solid State Phys. **18**, L371 (1985).
[16] C. A. Angell, Science **267**, 1924 (1995).
[17] M. Vogel and S. C. Glotzer, Phys. Rev. E **70**, 061504 (2004).
[18] D. Coslovich and G. Pastore, J. Phys.: Condens. Matter **21**, 285107 (2009).
[19] K. Kim and S. Saito, J. Chem. Phys. **138**, 12A506 (2013).
[20] H. Staley, E. Flenner, and G. Szamel, J. Chem. Phys. **143**, 244501 (2015).
[21] H. Shintani and H. Tanaka, Nat. Phys. **2**, 200 (2006).
[22] B. W. H. van Beest, G. J. Kramer, and R. A. van Santen, Phys. Rev. Lett. **64**, 1955 (1990).
[23] W. Kob and H. C. Andersen, Phys. Rev. E **48**, 4364 (1993).
[24] D. C. Rapaport, *The Art of Molecular Dynamics Simulation* (Cambridge University Press, Cambridge, 2004).
[25] K. Vollmayr, W. Kob, and K. Binder, Phys. Rev. B **54**, 15808 (1996).
[26] J. Horbach and W. Kob, Phys. Rev. B **60**, 3169 (1999).
[27] J. Horbach and W. Kob, Phys. Rev. E **64**, 041503 (2001).
[28] J. Horbach, W. Kob, and K. Binder, Eur. Phys. J. B **19**, 531 (2001).
[29] A. Saksaengwijit and A. Heuer, Phys. Rev. E **74**, 051502 (2006).
[30] I. Saika-Voivod, P. H. Poole, and F. Sciortino, Nature (London) **412**, 514 (2001).
[31] D. Wolf, Phys. Rev. Lett. **68**, 3315 (1992).
[32] A. Carré, L. Berthier, J. Horbach, S. Ispas, and W. Kob, J. Chem. Phys. **127**, 114512 (2013).
[33] The density field itself is a conservative variable; thus, at a large-enough length scales, the relaxation dynamics of density fluctuations should exhibit diffusive behavior. It is interesting to investigate at which size density diffusion can be recovered in the strong BKS silica, which requires future study.

[34] In the long-time limit ($\Delta t \gg \tau_\alpha$), $\boldsymbol{u}_i$ is independent of each other, and, thus, $H(k,\Delta t) = \langle|\boldsymbol{k}\cdot\hat{\boldsymbol{u}}_{\boldsymbol{k}}(\Delta t)|^2\rangle/N \cong 2D_s\Delta t k^2$, where D_s is the self-diffusion coefficient. However, for $\Delta t \sim \tau_\alpha$, because $\boldsymbol{u}_i$ is spatially correlated, the coefficient of k^2 is found to be larger than $2D_s\Delta t$ for smaller k.

[35] U. Buchenau, H. M. Zhou, N. Nucker, K. S. Gilroy, and W. A. Phillips, Phys. Rev. Lett. **60**, 1318 (1988).

[36] In the kinetic Ising model, the different elementary processes of the Glauber spin-flip and the Kawasaki spin-exchange dynamics result in *nonconserved* and *conserved* hydrodynamic relaxations of the (coarse-grained) order-parameter field, respectively [37]. Moreover, in fluid systems near criticality, the collective hydrodynamic effects dominate such microscopic processes.

[37] P. C. Hohenberg and B. I. Halperin, Rev. Mod. Phys. **49**, 435 (1977).

[38] At the time scale of the β relaxation, it has been pointed out that the density fluctuations are more strongly coupled with londitudinal vibrations in the strong glass formers than in fragile glass formers [39,40,41]. Our simulation results show that this is also the case even for time scale of the structural (α) relaxation.

[39] A. P. Sokolov, E. Rössler, A. Kisliuk, and D. Quitmann, Phys. Rev. Lett. **71**, 2062 (1993).

[40] E. Duval, T. Deschapms, and L. Savoit, J. Chem. Phys. **139**, 064506 (2013).

[41] U. Buchenau and A. Wischnewski, Phys. Rev. B **70**, 092201 (2004).

[42] V. N. Novikov and A. P. Sokolov, Nature **431**, 962 (2004).

[43] V. N. Novikov, Y. Ding, and A. P. Sokolov, Phys. Rev. E **71**, 061501 (2005).

[44] T. Rouxel, J. Am. Ceram. Soc. **90**, 3019 (2007).

[45] G. N. Greaves, A. L. Greer, R. S. Lakes, and T. Rouxel, Nat. Mater. **10**, 823 (2011).

[46] J. P. Hansen and I. R. McDonald, *Theory of Simple Liquids* (Academic Press, Oxford, 1986).

[47] J. P. Boon and S. Yip, *Molecular Hydrodynamics* (Dover, New York, 1991).

[48] For the two fragile models, we found that the self-diffusion coefficient of a tagged particle, D_s, is on the same order of magnitude as D_n (not shown in this paper): In normal states at higher temperatures, the particle dynamics are less-cooperative, resulting in the SE relation holding well. Such particle-scale dynamics dominate the hydrodynamic transport; thus, D_s determines D_n. However, in supercooled states at lower temperatures, the deviation from the SE relation is significant, which suggests that cooperative dynamics surpass particle-scale dynamics; thus, D_n determines D_s.